SANDIA REPORT

SAND2018-12274
Unlimited Release
Printed October 2018

Translation of Exterior Electromagnetic Environment to Pin-Level Voltages and Currents on Cables

Salvatore Campione, William L. Langston, and Larry K. Warne

Prepared by
Sandia National Laboratories
Albuquerque, New Mexico 87185 and Livermore, California 94550

Sandia National Laboratories is a multimission laboratory managed and operated by National Technology and Engineering Solutions of Sandia, LLC, a wholly owned subsidiary of Honeywell International, Inc., for the U.S. Department of Energy's National Nuclear Security Administration under contract DE-NA-0003525.

Issued by Sandia National Laboratories, operated for the United States Department of Energy by Sandia Corporation.

Available to DOE and DOE contractors from
U.S. Department of Energy
Office of Scientific and Technical Information
P.O. Box 62
Oak Ridge, TN 37831

Telephone: (865) 576-8401
Facsimile: (865) 576-5728
E-Mail: reports@osti.gov
Online ordering: http://www.osti.gov/scitech

Available to the public from
U.S. Department of Commerce
National Technical Information Service
5301 Shawnee Rd
Alexandria, VA 22312

Telephone: (800) 553-6847
Facsimile: (703) 605-6900
E-Mail: orders@ntis.gov
Online order: http://www.ntis.gov/search

SAND2018-12274
Unlimited Release
Printed October 2018

Translation of Exterior Electromagnetic Environment to Pin-Level Voltages and Currents on Cables

Salvatore Campione, William L. Langston, and Larry K. Warne
Electromagnetic Theory

Sandia National Laboratories
P.O. Box 5800
Albuquerque, New Mexico 87185-1152

Abstract

This report explores the coupling between EIGER simulations and a transmission line analytical model to enable end-to-end simulations to translate an exterior electromagnetic environment to assess effects on electronic system performance.

Intentionally Left Blank

CONTENTS

FIGURES

TABLES

1. INTRODUCTION

The purpose of this report is to explore the coupling between EIGER simulations [1-3] and a transmission line (TL) analytical model [4] to enable end-to-end simulations to translate an exterior electromagnetic (EM) environment to assess effects on electronic system performance.

We focus on the simple test case of a canonical slotted cylindrical cavity containing a braided shield cable, excited by an external EM threat. EIGER simulations account for the coupling problem (through the slot) to find the interior fields of the cavity due to the external excitation. These interior fields induce currents on the shield of the cable lying within the cavity, which are readily computed with EIGER. Since the shields are not perfect conductors and apertures in the shields permit external magnetic and electric fields to penetrate into the interior regions of the cable, we use a TL model to estimate the effects of the outer shield current and charge (associated with the external excitation and boundary conditions of the external conductor) on the current and voltage associated with the inner conductor. These inner conductor currents and voltages can then be used as inputs of circuit simulations to predict failures, damage, etc. of electronics within the cavity.

2. DEFINITION OF THE TEST CAVITY STRUCTURE UNDER ANALYSIS

We introduce the geometry that will be used for the remainder of this report, namely a 0.25 inch thick aluminum cylinder ($\sigma = 2.6\times10^7$ S/m) with interior height $h = 0.6096$ m and interior radius $a = 0.1016$ m, with a 0.02 inch (width) x 2 inch (length) slot on one side of the cylinder located midway along the cylinder length as shown in Figure 1(a). This cavity is excited by an external threat modeled as a plane wave source propagating along the –*x*-direction and with electric field along the *z*-direction. Note that the slot resonates at $f_{\text{slot}} = \dfrac{c}{2l_{\text{slot}}} = \dfrac{3\times10^8}{0.1016} \approx 2.95$ GHz, so that, at the frequencies analyzed in this report, its purpose is to provide a magnetic current source drive for the interior cavity modes from the exterior fields.

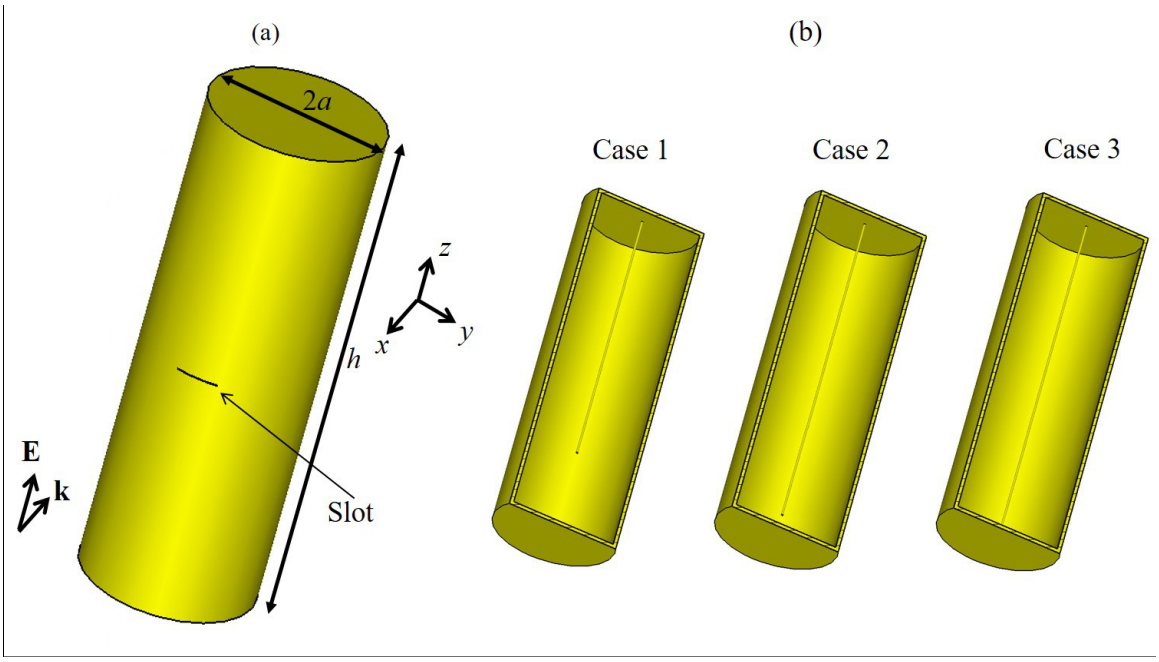

Figure 1. (a) Schematic of a 0.25 inch thick cylindrical cavity with a small 0.02 inch (width) x 2 inch (length) slot being excited by a plane-wave incident field with electric field along the *z*-direction. (b) Schematics of Cases 1-3 comprising one single-shield cable at the center of the cavity: Case 1: 18 inch; Case 2: 23.75 inch; Case 3: 24 inch.

We consider three different length and termination configurations for three braided-shield commercial cables (REMEE, Belden 9201, Belden 8240) located in the middle of the cavity as detailed in Figure 1(b) (a total of nine combinations). The three different length configurations are referred to as 'Case 1', 'Case 2', and 'Case 3'. Case 1 has an 18 inch long cable whose shield is short circuited on one side to the top plate of the cylinder; Case 2 has a 23.75 inch long cable whose shield is short circuited on one side to the top plate of the cylinder (this configuration may increase the transfer admittance contribution because of the capacitive effect of the 0.25 inch

gap); Case 3 has a 24 inch long cable whose shield is short circuited on both sides to the bottom and top plates of the cylinder. We use the geometrical parameters listed in Table 1 and Table 2 for REMEE, Belden 9201, and Belden 8240 cables.

Table 1. Geometrical parameters for REMEE, Belden 9201, and Belden 8240 cables.

Parameter	REMEE	Belden 9201	Belden 8240
Wires per strip	3	5	7
Braid angle (degrees)	34.2	22	24.4
Braid outer diameter, max (inches)	0.1394	0.13	0.134

Table 2. Braid parameters common to REMEE, Belden 9201, and Belden 8240 cables.

Parameter	Braid
Number of strips	16
Metal conductivity (S/m)	5.8×10^{7}
Wire diameter (inches)	0.005
Braid inner diameter (inches)	0.116
Diameter of core insulator (inches)	0.116
Inner conductor diameter (inches)	0.033
Outer jacket diameter (inches)	0.193
Interior relative permittivity to braid, PVC	2.3
Exterior relative permittivity to braid, polyethylene	3.3
Average relative permittivity of interior insulation	2.3

We assume a unit external electric field $E_0 = 1$ V/m, and use EIGER simulations to compute the current profiles induced on the shield of the cable within the cavity (the charge information is subsequently computed as the derivative of the current with respect to the spatial direction along the cable). Because fields penetrate through the cable shield, we use the TL model reported in Appendix A to compute the inner conductor current and voltage profiles for various loading conditions of the inner conductor. Then, we define transfer functions as

$$T_I(z) = \frac{I_c(z)}{E_0} \tag{1}$$

in units of $\mathrm{A}/(\mathrm{V/m})$ (from the current) and

$$T_V(z) = \frac{V_c(z)}{E_0} \tag{2}$$

in units of m (from the voltage, defining an effective height) between cable inner conductor currents and voltages and E_0.

These transfer functions could then be used as inputs of circuit simulations to predict failures, damage, etc. of circuitry within the cavity. To have the correct response from an insult with a

given field strength, the results here reported should be scaled by the strength of the threat (for example, for EM radiation, the values reported can be scaled by the threats given in the MIL-STD-464C document).

3. TRANSMISSION LINE MODEL TO CONNECT EIGER SIMULATIONS TO CIRCUIT SIMULATIONS

In this section, we use the TL code in Appendix A, with shield currents coming from EIGER simulations, for the three cases in Figure 1, and compute current and voltages induced in the inner conductor of the cable for various terminations of the inner conductor, through which we compute the transfer functions in Eqs. (1) and (2). The three commercial cables differ for the level of optical coverage (from low to high): REMEE (59%), Belden 9201 (78%), and Belden 8240 (95%).

We take the simulation parameters to be $Z_T = Z_R + j\omega L_T + Z_S$, where $Z_R = R_{gs}\dfrac{\gamma d_R}{\sin(\gamma d_R)}$ accounts for the shield diffusion effect, with $\gamma = \dfrac{1-j}{\delta}$, $\delta = \sqrt{\dfrac{2}{\omega\mu_0\sigma}}$ the skin depth, R_{gs} accounts for the losses in the shield, $Z_S = (1+j)\omega L_S$ is the internal transfer impedance assumed to be a 45° phasor quantity, $Y_T = j\omega C_T$. The inner conductor self-impedance and admittance are given by $Z_c = R + j\omega L_c$ and $Y_c = j\omega C_c$, respectively, with $L_c = \dfrac{\mu_0}{2\pi}\log\dfrac{b+r}{a}$, with b the braid inner radius, r the wire radius, and a the inner conductor radius, and $C_c = \dfrac{2\pi\varepsilon_0\varepsilon_1}{\log\dfrac{b+r}{a}}$, and $R = 0.43\sqrt{\omega/\omega_0}$, with $\omega_0 = 2\pi\times 10\times 10^6$ rad/s.

3.1. Case 1: 18-inch long cable

We consider here various loading examples of the inner conductor. The top end of the shield is short-circuited to the top surface of the cylinder, while the bottom end is left open-circuited, thus the 18 inch long cable resonates at $f_{\text{cable}} = \dfrac{c}{4l_{\text{cable}}} = \dfrac{3\times 10^8}{1.8288} \approx 164$ MHz. In EIGER, the shield is assumed to be made of copper with $\sigma = 5.8\times 10^7$ S/m.

3.1.1 Transfer parameters for short-circuited inner conductor

We assume that the inner conductor is short-circuited at both ends. We plot in Figure 2 the transfer parameter T_I at the two ends of the inner conductor for the three cables REMEE, Belden 9201, and Belden 8240, where we also investigate the effect of the transfer admittance Y_T. One can readily observe that the REMEE exhibits the worst performance among the three cables, for which $T_I \approx 10^{-5}$ A/(V/m) at resonance. We expect Y_T not to play a role in the Belden 8240, as confirmed by Figure 2(c), while it does play a role in the other two cables. We know that $I_c(z) = I_{c,e}(z) + I_{c,j}(z)$ (see Appendix A for the definition of the individual current components); for the Belden 9201, the two individual contributions of electric and magnetic

currents are in phase at the two ends of the cable so that when Y_T is present the transfer parameter T_I is larger than without Y_T (see Figure 2(b)). However, for the REMEE, the two individual contributions are in phase at one end and out of phase at the other end of the cable, so that when Y_T is present the transfer parameter T_I is larger than without Y_T at one end and smaller than without Y_T at the other end (see Figure 2(a)).

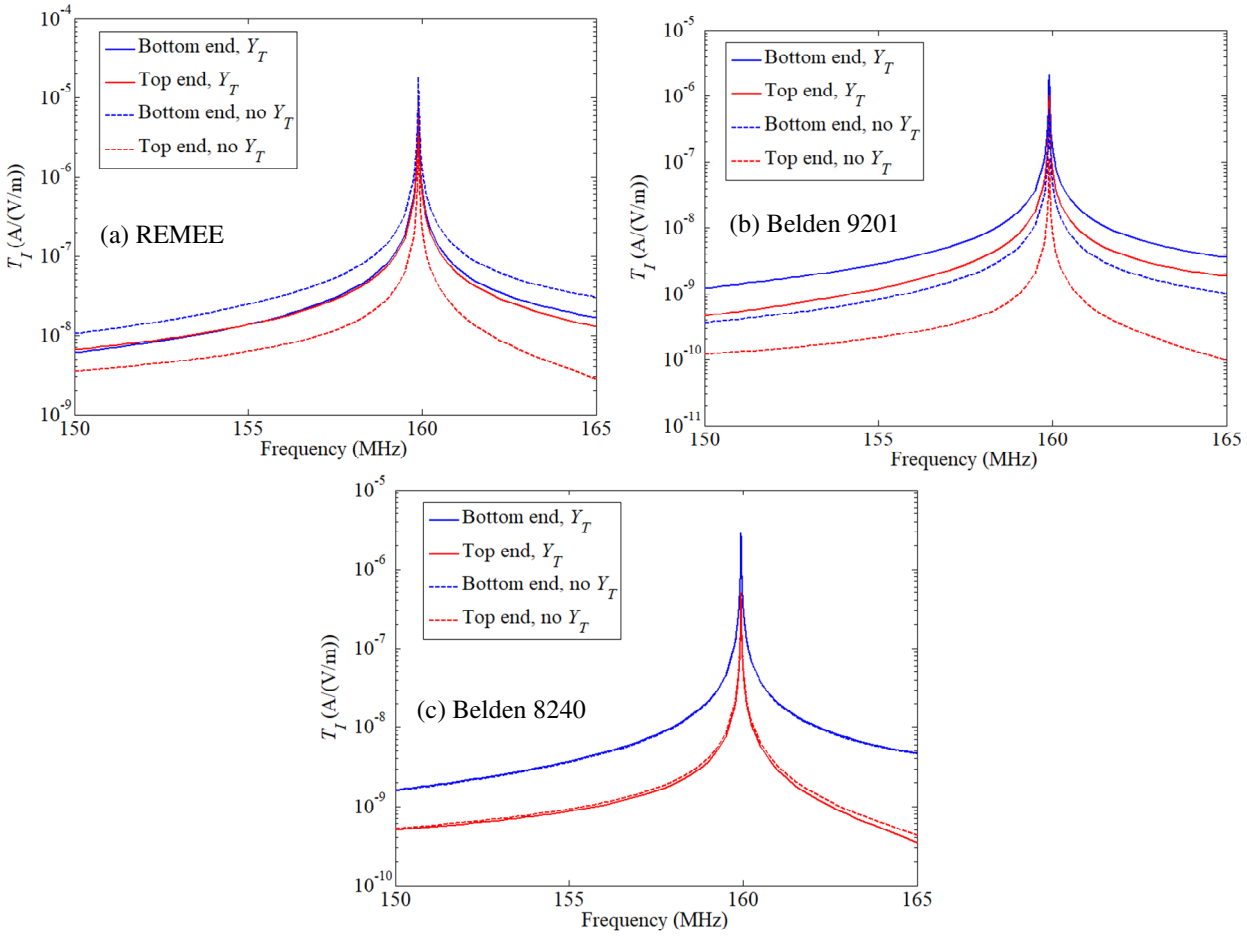

Figure 2. Transfer parameter T_I spectrum at the two ends of the 18 inch cable for (a) REMEE, (b) Belden 9201, and (c) Belden 8240. The effect of the transfer admittance Y_T is investigated. The inner conductor terminations are short circuits.

We then plot in Figure 3 the shield and inner conductor transfer parameter T_I profiles as well as the inner conductor transfer parameter T_V profile along the cable at the resonance frequency in Figure 2. While the currents on the shields of the three cables are very similar (as they come from EIGER, where the only variations include the diameters of the shield according to Table 1), the inner conductor transfer parameter T_I and T_V exhibit different profiles due to the different braided shield properties.

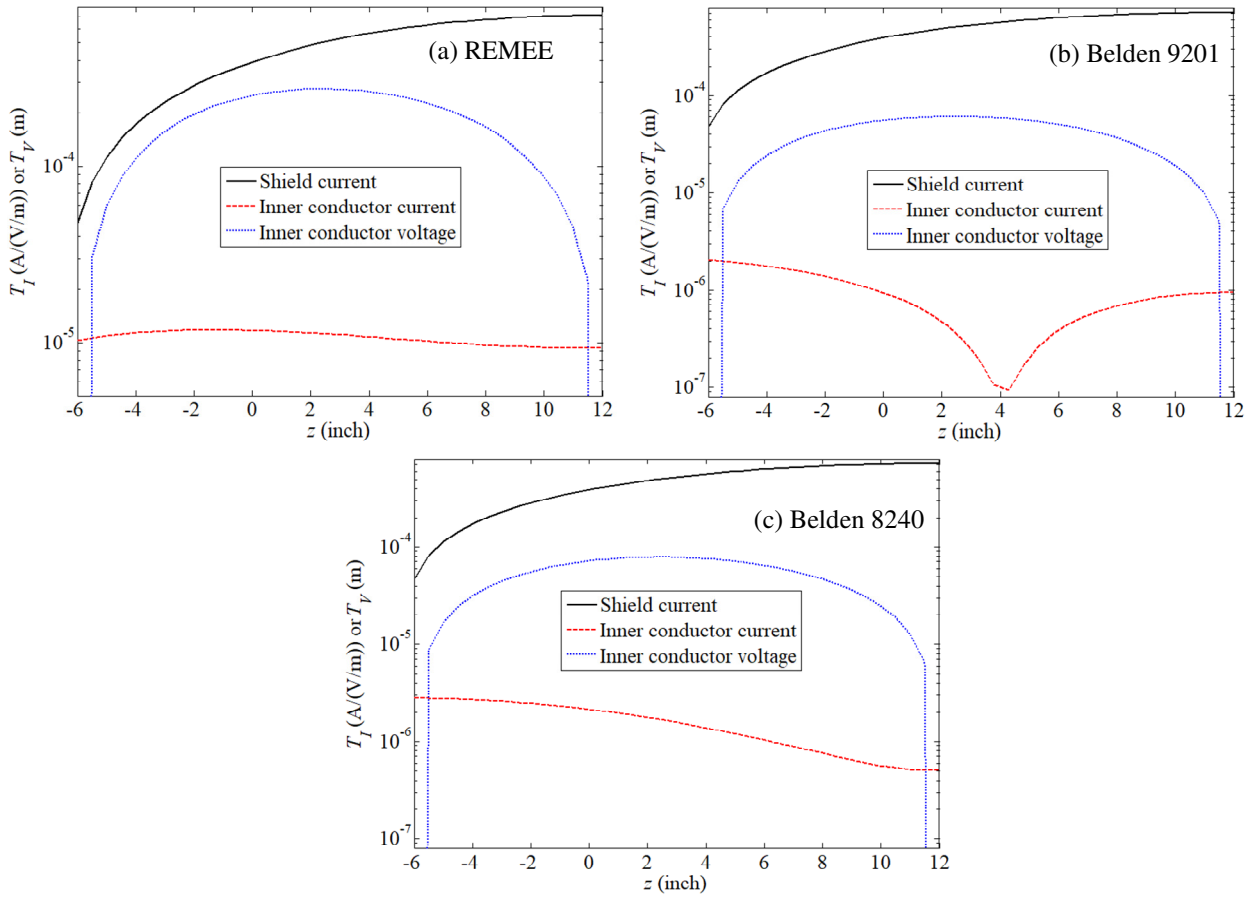

Figure 3. Shield and inner conductor transfer parameters T_I and T_V profiles along the 18 inch cable at the resonance in Figure 2 for (a) REMEE, (b) Belden 9201, and (c) Belden 8240. The inner conductor terminations are short circuits.

3.1.2 Transfer parameters for inner conductor terminated to 50 Ohm loads

We assume that the inner conductor is terminated in 50 Ohm loads at both ends. We plot in Figure 4 the transfer parameter T_V versus frequency at the two ends of the inner conductor for the three cables REMEE, Belden 9201, and Belden 8240. One can readily observe again that the REMEE exhibits the worst performance among the three cables, for which $T_V \approx 4.5\times10^{-4}$ m at resonance.

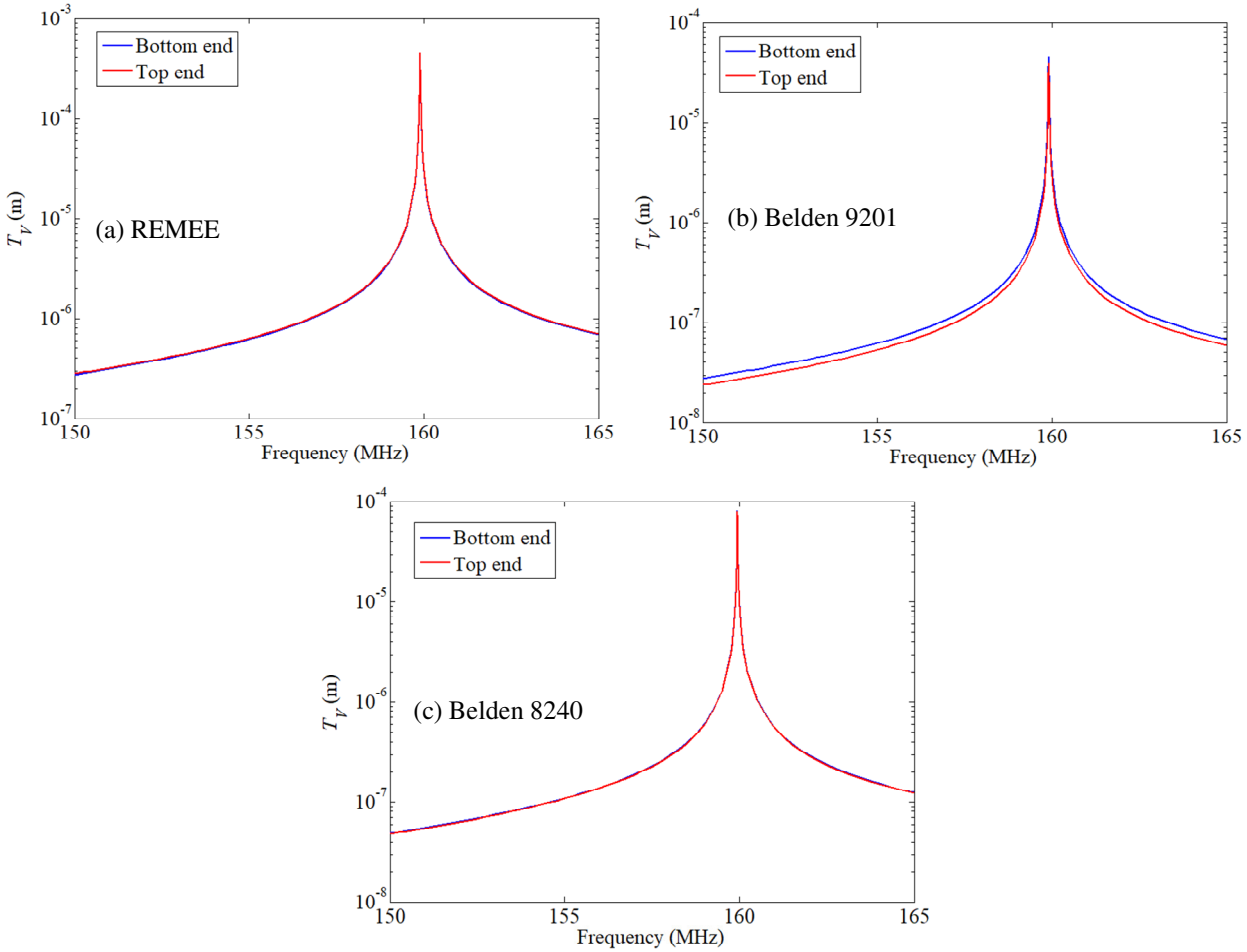

Figure 4. Transfer parameter T_V spectrum at the two ends of the 18 inch cable for (a) REMEE, (b) Belden 9201, and (c) Belden 8240. The inner conductor terminations are 50 Ohm loads.

We then plot in Figure 5 the shield and inner conductor transfer parameter T_I profiles as well as the inner conductor transfer parameter T_V profile along the cable at the resonance frequency in Figure 4. While the currents on the shields of the three cables are very similar (as they come from EIGER, where the only variations include the diameters of the shield according to Table 1), the inner conductor currents and voltages exhibit different profiles due to the different braided shield properties.

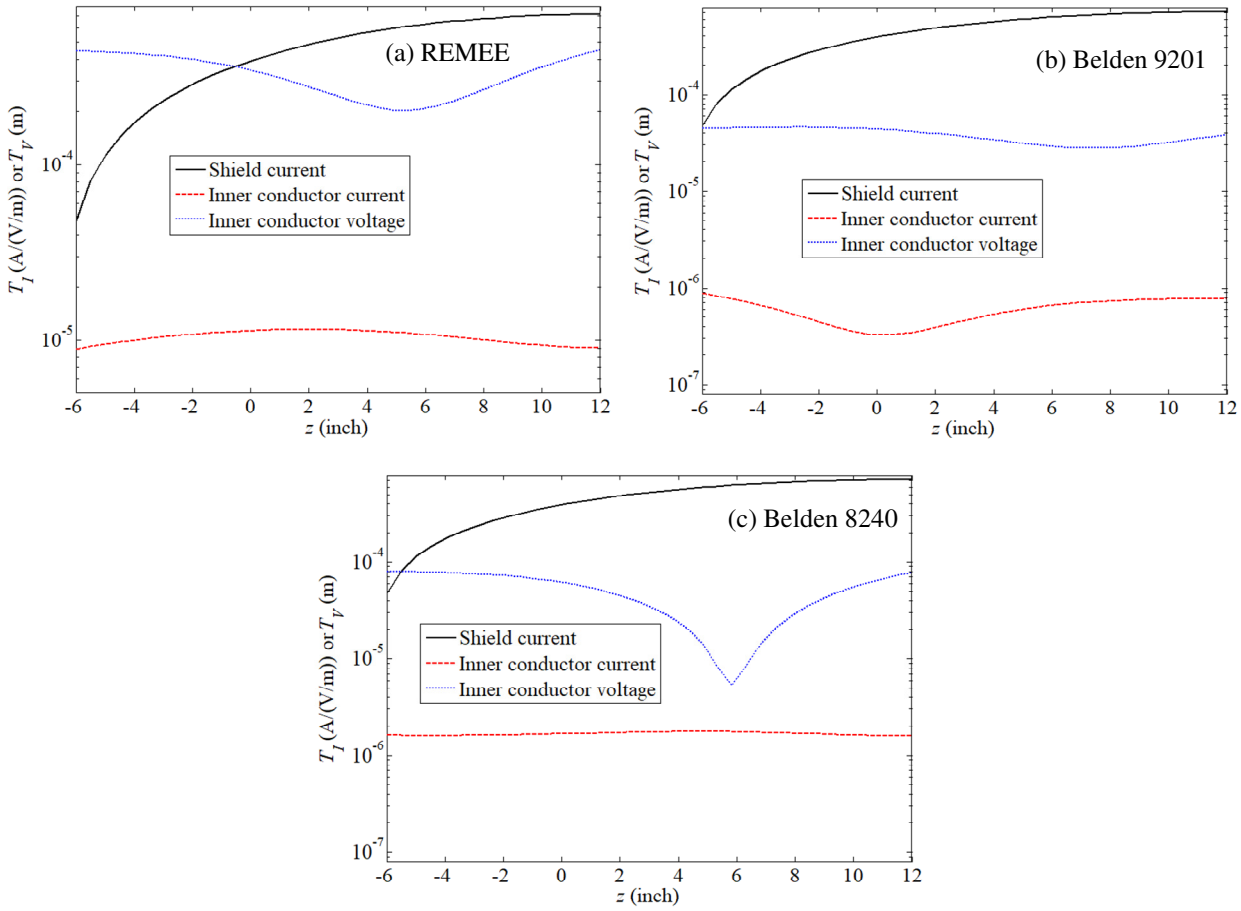

Figure 5. Shield and inner conductor transfer parameters T_I and T_V profiles along the 18 inch cable at the resonance in Figure 5 for (a) REMEE, (b) Belden 9201, and (c) Belden 8240. The inner conductor terminations are 50 Ohm loads.

3.1.3 Transfer parameters for inner conductor terminated to a 50 Ohm load on one side and left open-circuited on the other

We assume that the inner conductor is terminated in a 50 Ohm load at the top inner conductor termination, and is left open-circuited at the bottom termination. We plot in Figure 6 the transfer parameter T_V versus frequency at the two ends of the inner conductor for the three cables REMEE, Belden 9201, and Belden 8240. At resonance, the inner conductor transfer parameter for the REMEE reaches values of $T_V \approx 9\times10^{-4}$ m ; for an external threat with field strength of, for example, 10000 V/m, the voltage induced at the termination is 9 V.

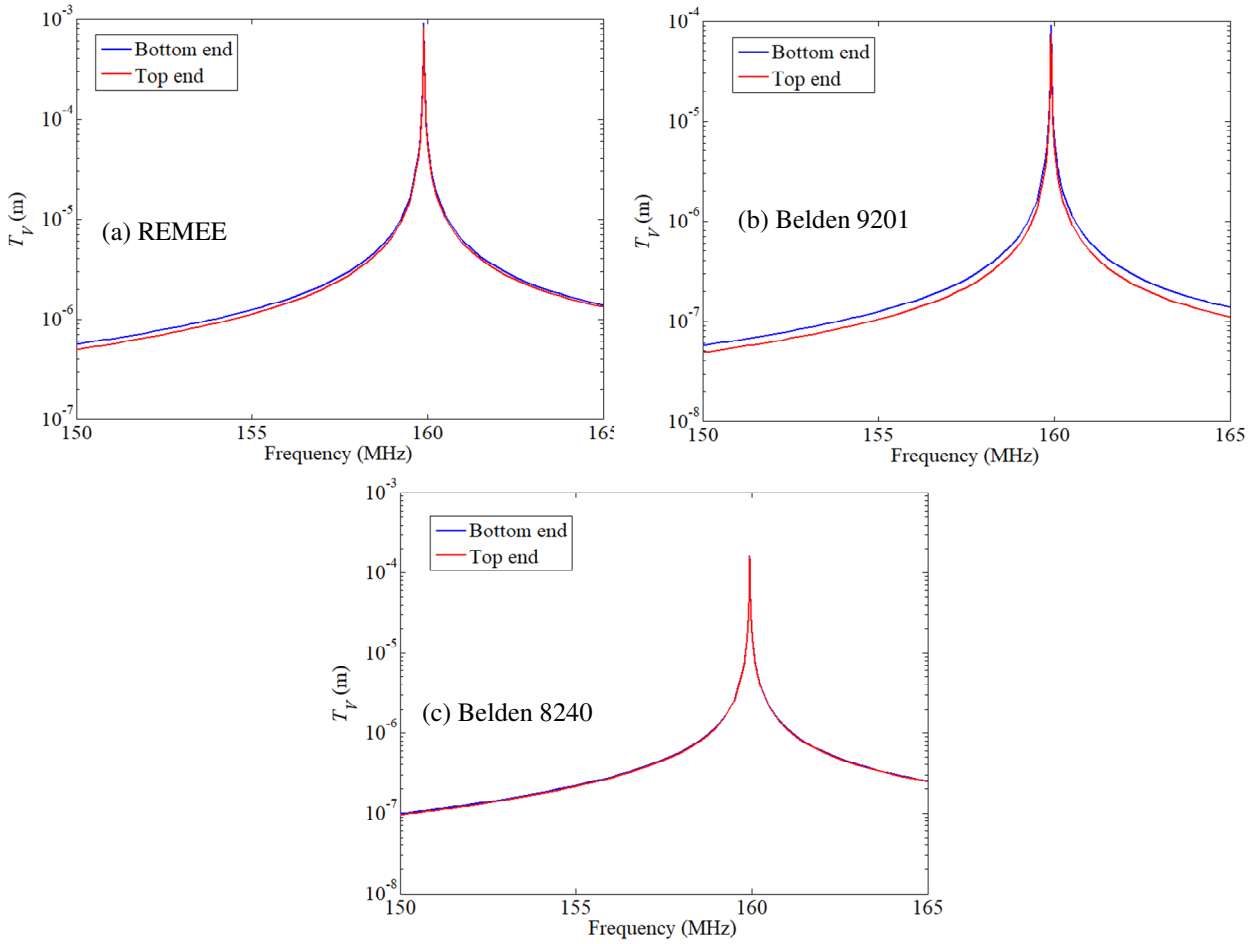

Figure 6. Transfer parameter T_V spectrum at the two ends of the 18 inch cable for (a) REMEE, (b) Belden 9201, and (c) Belden 8240. The inner conductor terminations are a 50 Ohm load at the top and an open circuit at the bottom.

We now introduce a capacitive load in place of the 50 Ohm load, while keeping the other end open circuited. We thus plot in Figure 7 the transfer parameter T_V versus frequency at the two ends of the inner conductor for the three cables REMEE, Belden 9201, and Belden 8240 when using a termination capacitance of 48 nF; at resonance, the inner conductor transfer parameter reaches values of $T_V \approx 9\times10^{-2}$ m for the REMEE and $T_V \approx 1.75\times10^{-2}$ m for the Belden 8240; for an external threat with field strength of 10000 V/m, the voltage induced at the termination is 900 V and 175 V, respectively.

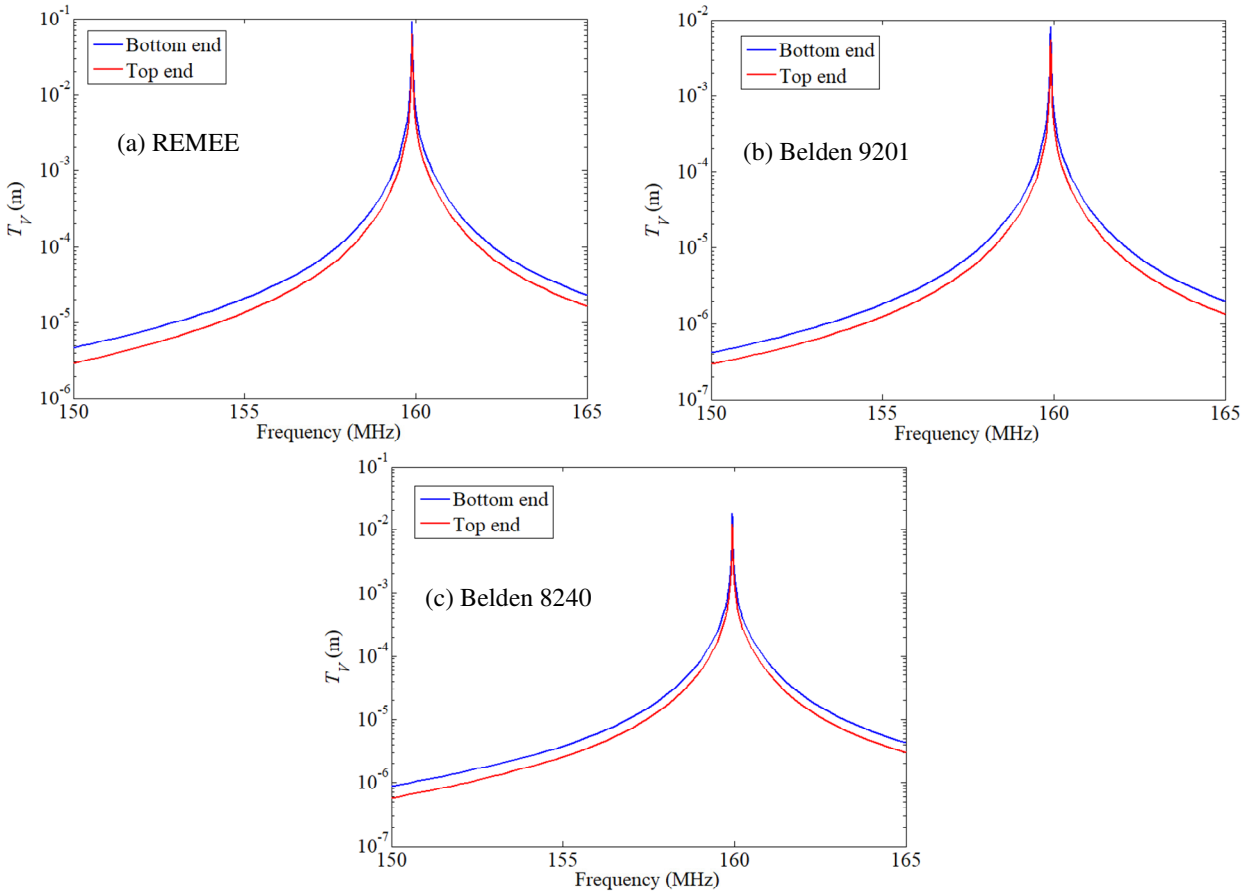

Figure 7. Transfer parameter T_V spectrum at the two ends of the 18 inch cable for (a) REMEE, (b) Belden 9201, and (c) Belden 8240. The inner conductor terminations are a 48 nF capacitive load at the top and an open circuit at the bottom.

3.2. Case 2: 23.75-inch long cable

The top end of the shield is short-circuited to the top surface of the cylinder, while the bottom end is left open-circuited, thus the 23.75 inch long cable resonates at $f_{\text{cable}} = \dfrac{c}{4l_{\text{cable}}} = \dfrac{3\times10^8}{2.413} \approx 124$ MHz. This resonance will be affected by the 0.25 inch capacitive gap. In EIGER, the shield is assumed to be made of copper with $\sigma = 5.8\times10^7$ S/m.

3.2.1 Transfer parameters for short-circuited inner conductor

We assume that the inner conductor is short-circuited at both ends. We plot in Figure 8 the transfer parameter T_I at the two ends of the inner conductor for the three cables REMEE, Belden 9201, and Belden 8240, where we also investigate the effect of the transfer admittance Y_T. One can readily observe that the REMEE exhibits the worst performance among the three cables, for

which $T_I \approx 10^{-5}$ A/(V/m) at resonance. We expect Y_T to play a bigger role here than in the 18 inch wire of the previous subsection (compare Figure 8 to Figure 2); this is because the fields in the 0.25 inch gap are contributing to the overall capacitive effects.

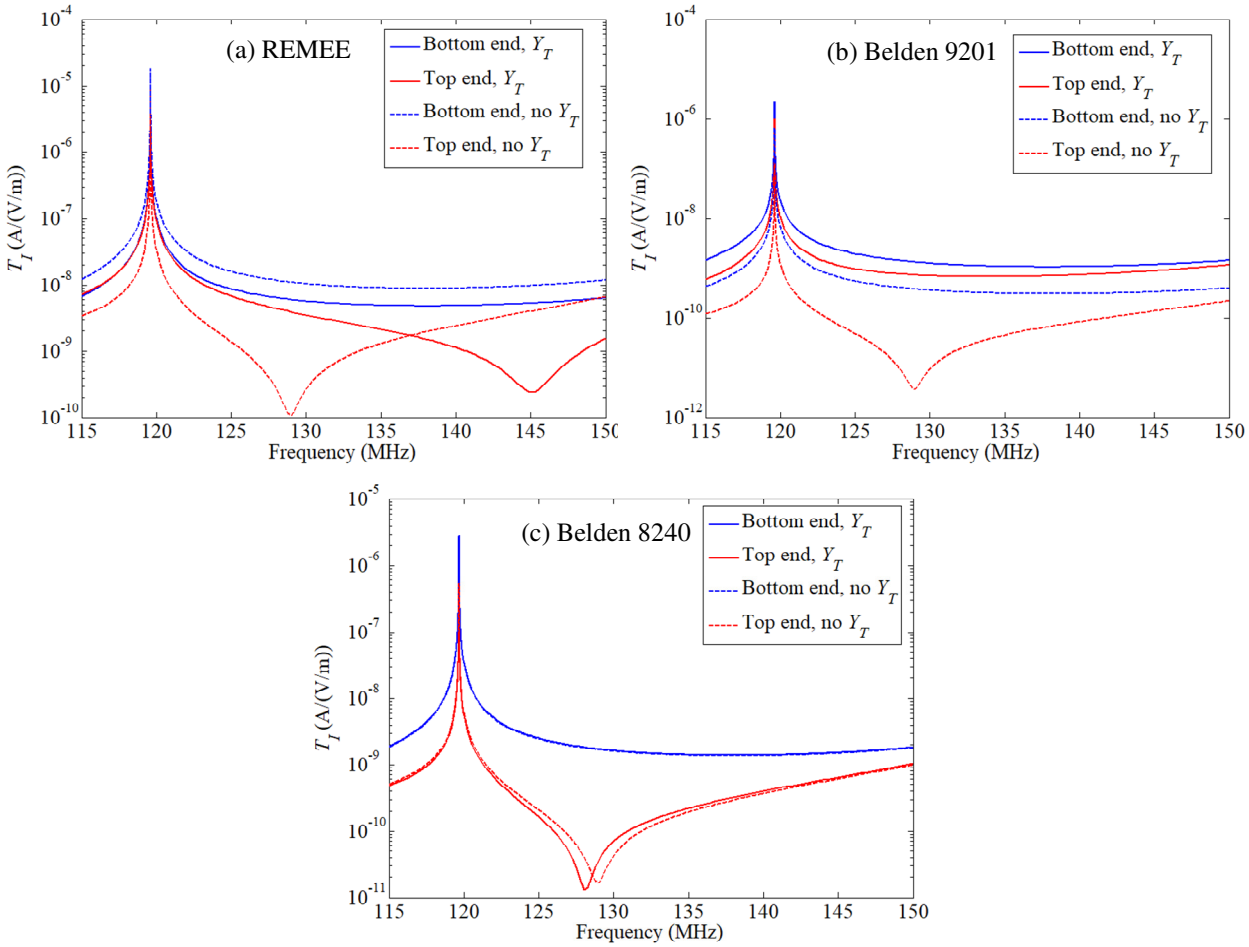

Figure 8. Transfer parameter T_I spectrum at the two ends of the 23.75 inch cable for (a) REMEE, (b) Belden 9201, and (c) Belden 8240. The effect of the transfer admittance Y_T is investigated. The inner conductor terminations are short circuits.

We now introduce an open circuit in place of the short circuit at the top termination, while keeping the other end short circuited; we also consider the permittivity of the inner region of the cable $\varepsilon_1 = 1.08$ (instead of 2.3) in this case. We thus plot in Figure 9 the transfer parameters T_V (at the open circuit) and T_I (at the short circuit) versus frequency for the three cables REMEE, Belden 9201, and Belden 8240; at resonance, the inner conductor transfer parameters reach values of $T_V \approx 1.27\times10^{-1}$ m and $T_I \approx 1.7\times10^{-3}$ A/(V/m) for the REMEE; for an external threat with field strength of 10000 V/m, the voltage and current induced at the terminations are 1270 V and 17 A, respectively. For the Belden 8240, the inner conductor transfer parameters reach

values of $T_V \approx 1.56\times10^{-2}$ m and $T_I \approx 2.1\times10^{-4}$ A/(V/m); for an external threat with field strength of 10000 V/m, the voltage and current induced at the terminations are 156 V and 2.1 A, respectively.

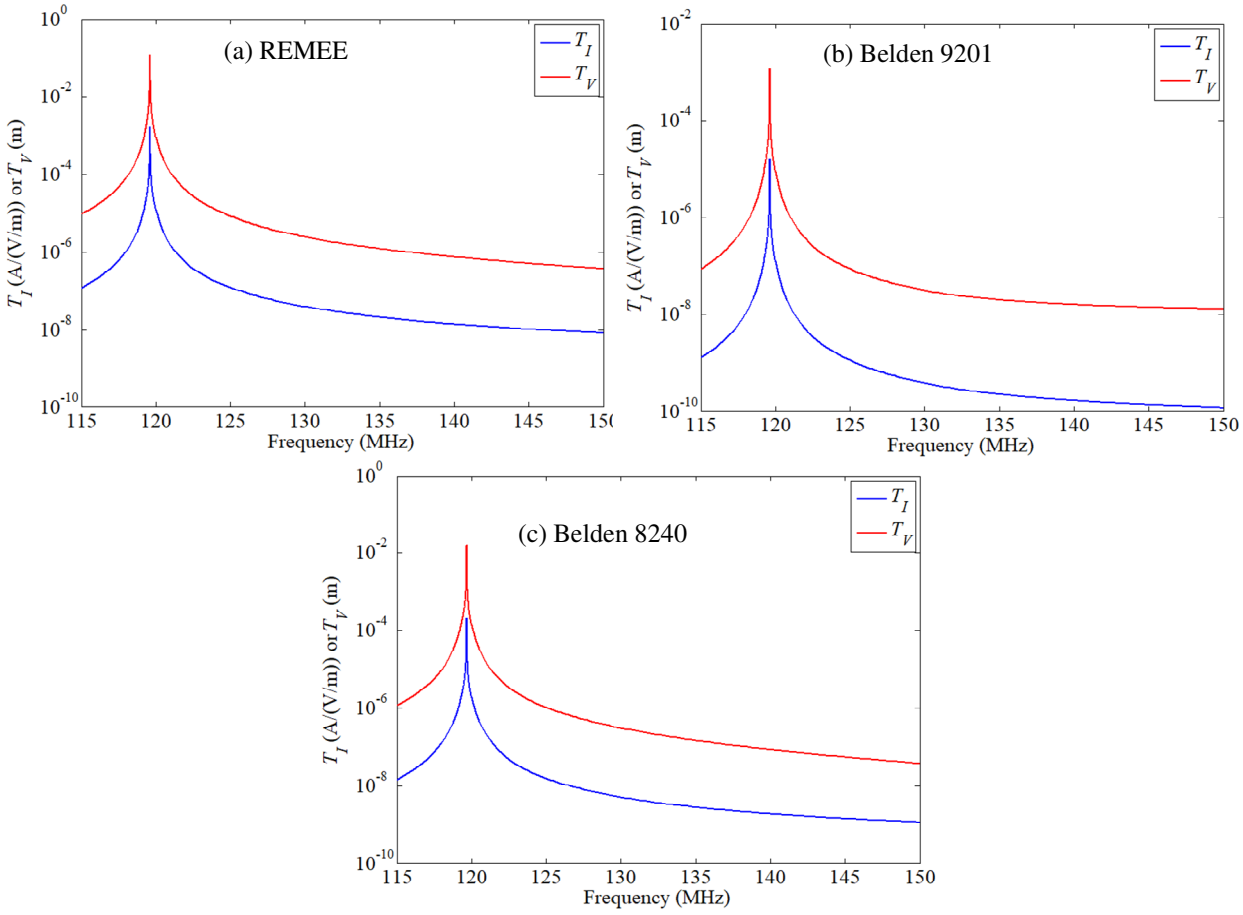

Figure 9. Transfer parameter T_V (at the open circuit) and T_I (at the short circuit) spectrum of the 23.75 inch cable for (a) REMEE, (b) Belden 9201, and (c) Belden 8240. The inner conductor terminations are an open circuit at the top and a short circuit at the bottom. The permittivity of the inner region of the cable is $\varepsilon_1 = 1.08$ (instead of 2.3).

3.2.2 Transfer parameters for inner conductor terminated to a 50 Ohm load on one side and left open-circuited on the other

We assume that the inner conductor is terminated in a 50 Ohm load at the top inner conductor termination, and is left open-circuited at the bottom termination. We plot in Figure 10 the transfer parameter T_V versus frequency at the two ends of the inner conductor for the three cables REMEE, Belden 9201, and Belden 8240. At resonance, the inner conductor transfer

parameter for the REMEE reaches values of $T_V \approx 9\times10^{-4}$ m; for an external threat with field strength of 10000 V/m, the voltage induced at the termination is 9 V.

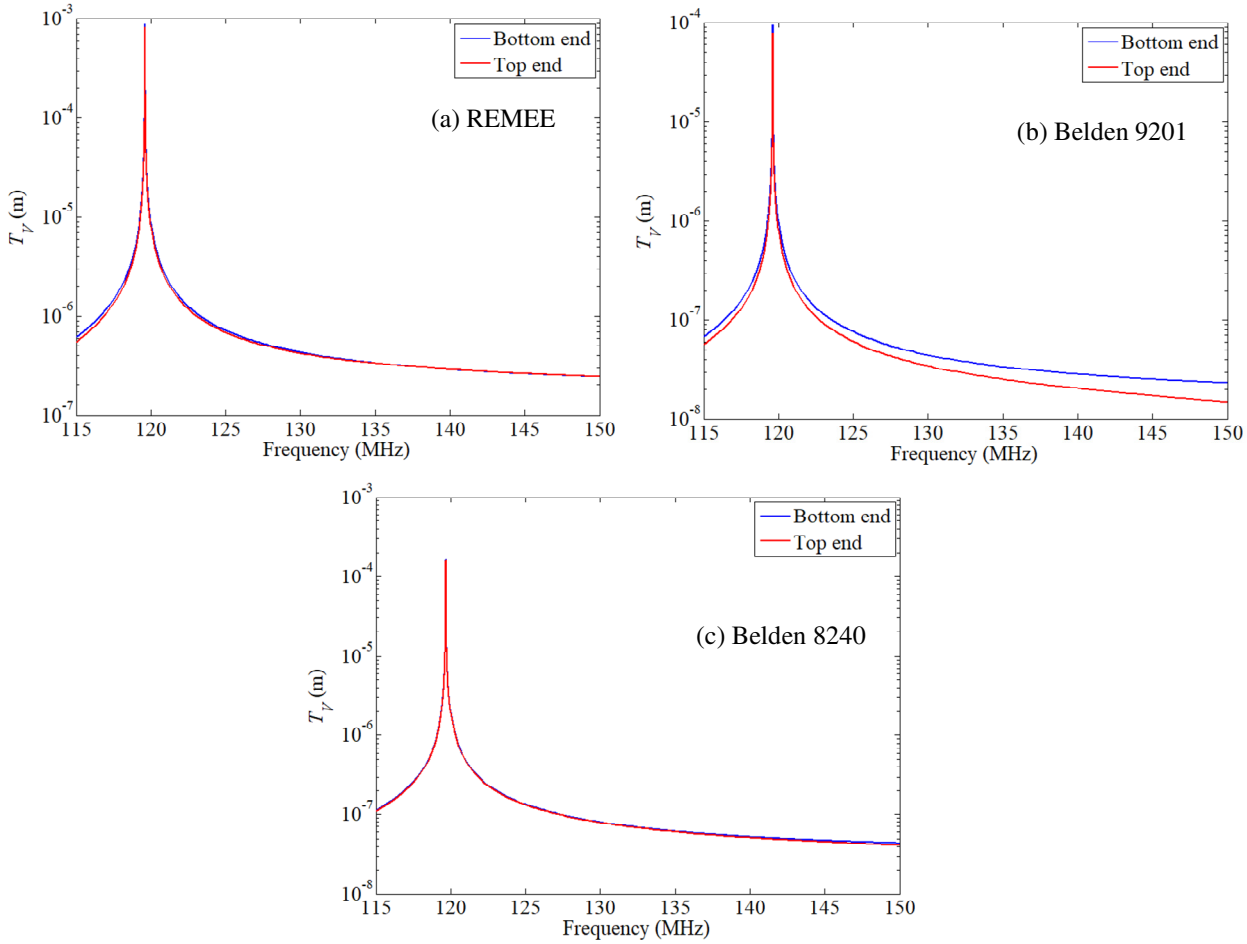

Figure 10. Transfer parameter T_V spectrum at the two ends of the 23.75 inch cable for (a) REMEE, (b) Belden 9201, and (c) Belden 8240. The inner conductor terminations are a 50 Ohm load at the top and an open circuit at the bottom.

3.3. Case 3: 24-inch long cable

Both ends of the shield are short-circuited to the top and bottom surfaces of the cylinder, thus the 24 inch long cable resonates at $f_{\text{cable}} = \dfrac{c}{2l_{\text{cable}}} = \dfrac{3\times10^8}{1.2192} \approx 246$ MHz. We will analyze here the second cable resonance of 492 MHz. In EIGER, the shield is assumed to be made of copper with $\sigma = 5.8\times10^7$ S/m.

3.3.1 Voltage for open-circuited inner conductor

We assume that the inner conductor is open-circuited at both ends. We plot in Figure 11 the transfer parameter T_V versus frequency at the two ends of the inner conductor for the three cables REMEE, Belden 9201, and Belden 8240. At resonance, the inner conductor transfer parameter for the REMEE reaches values of $T_V \approx 4\times10^{-3}$ m; for an external threat with field strength of 10000 V/m, the voltage induced at the termination is 40 V.

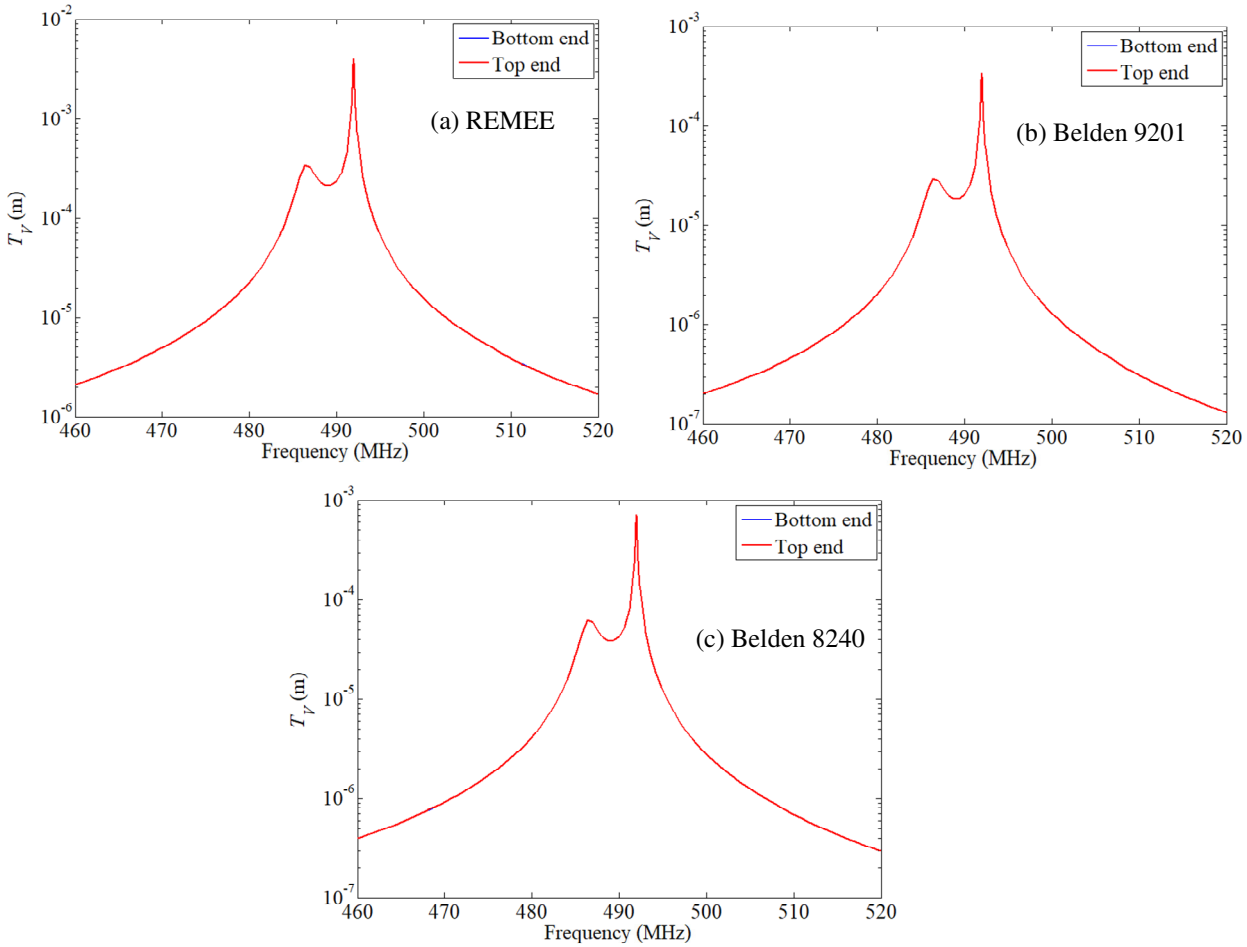

Figure 11. Transfer parameter T_V spectrum at the two ends of the 24 inch cable for (a) REMEE, (b) Belden 9201, and (c) Belden 8240. The inner conductor terminations are open circuits.

We now change the permittivity of the inner region of the cable ε_1 to 2.25 (instead of 2.3), so that the second resonance at lower frequency observed in Figure 11 aligns with the major peak. We then plot in Figure 12 the transfer parameter T_V versus frequency at the two ends of the inner conductor for the three cables REMEE, Belden 9201, and Belden 8240; at resonance, the inner conductor transfer parameter reaches values of $T_V \approx 2.5\times10^{-2}$ m for the REMEE cable; for an external threat with field strength of 10000 V/m, the voltage induced at the termination is 250 V. Similarly, the inner conductor transfer parameter reaches values of $T_V \approx 4.5\times10^{-3}$ m for the

Belden 8240 cable; for an external threat with field strength of 10000 V/m, the voltage induced at the termination is 45 V.

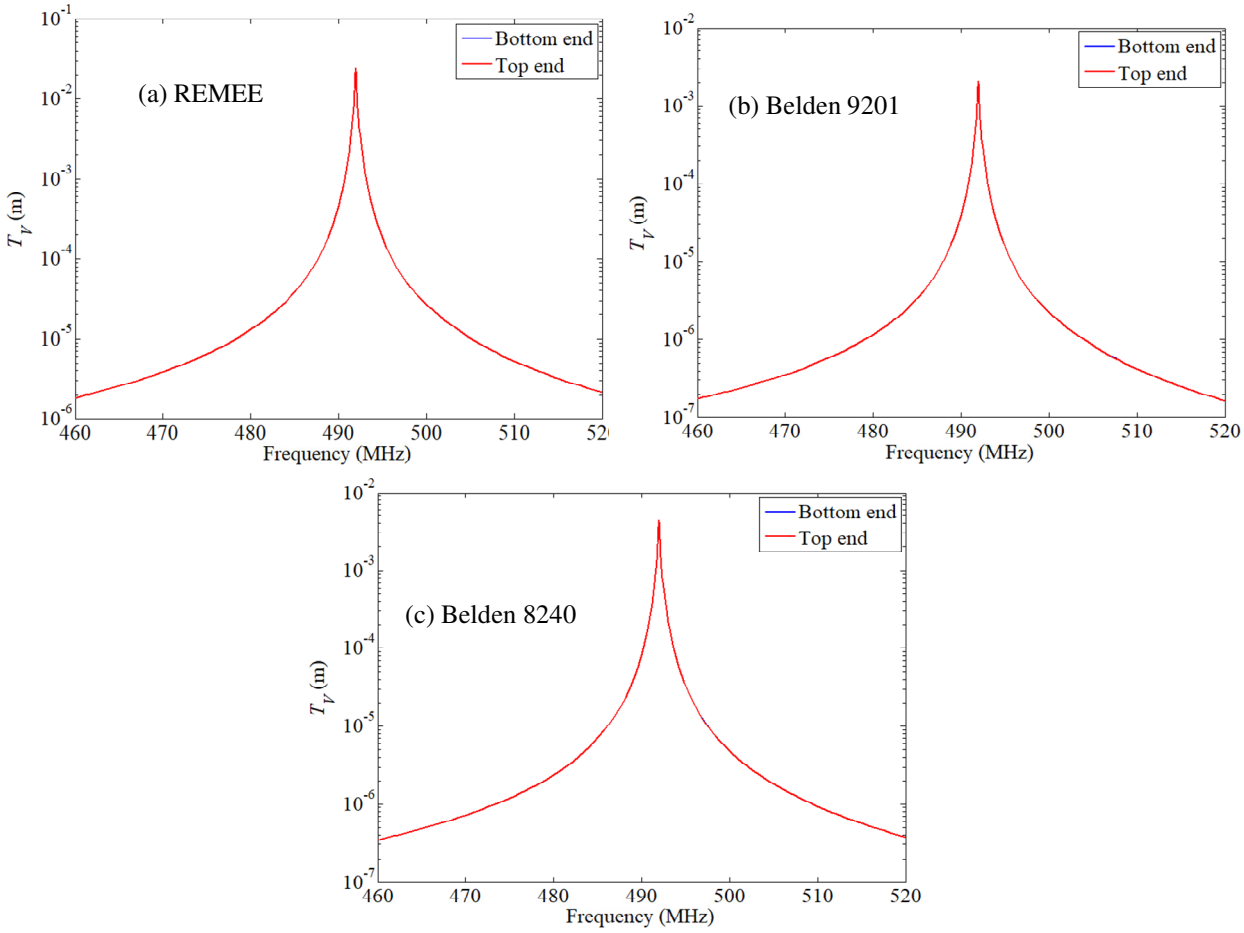

Figure 12. Transfer parameter T_V spectrum at the two ends of the 24 inch cable for (a) REMEE, (b) Belden 9201, and (c) Belden 8240. The inner conductor terminations are open circuits. The permittivity of the inner region of the cable is $\varepsilon_1 = 2.25$ (instead of 2.3).

4. CONCLUSIONS

In this report we investigated the coupling between EIGER simulations of resonant cavities comprising cables and transmission line (TL) analytic models to enable end-to-end simulations to translate the exterior environment to an assessment on the electronic system performance.

We observed that different cable loading conditions results in very different values of inner conductor transfer parameter T_I and T_V. These inner conductor parameters could then be scaled by a given threat strength to predict or evaluate failures, damage, etc. of circuitry within the cavity.

REFERENCES

[1] D. R. Wilton, W. A. Johnson, R. E. Jorgenson, R. M. Sharpe, and J. B. Grant, "EIGER: A new generation of computational electromagnetics tools," retrieved from http://www.osti.gov/scitech/servlets/purl/219454 (1996).
[2] R. M. Sharpe, J. B. Grant, N. J. Champagne, W. A. Johnson, R. E. Jorgenson, D. R. Wilton, W. J. Brown, and J. W. Rockway, "EIGER: Electromagnetic Interactions GEneRalized," retrieved from http://www.osti.gov/scitech/servlets/purl/501495 (1997).
[3] EIGER, https://pulsedpower.sandia.gov/ppt_tech/compphys/Projects/eiger/eiger.html - 2017.
[4] S. Campione, L.I. Basilio, L.K. Warne, H.G. Hudson, and W.L. Langston, "Shielding effectiveness of multiple-shield cables with arbitrary terminations via transmission line analysis," *Progress in Electromagnetics Research C* **65**, 93-102 (2016).

APPENDIX A: TRANSMISSION LINE MODEL OF SINGLE-SHIELD CABLES

In order to model a shielded cable, we consider an element of transmission line of differential length *dz* that contains a distributed voltage source $E_z(z) = Z_T I_0(z)$, where $I_0(z)$ is the current on the outer shield, as well as a distributed current source $J_z(z) = -Y_T V_0(z)$, where $V_0(z)$ is the external voltage on the outer shield. This Appendix summarizes the formulation reported in [4], where the reader is directed for more details on the subject.

The differential equations for the voltage and current on the inner conductor of the braided cable (V_c and I_c) are given by

$$\frac{dV_c}{dz} + Z_c I_c = Z_T I_0(z) \qquad \frac{dI_c}{dz} + Y_c V_c = -Y_T V_0(z). \tag{A.1}$$

where the shield properties (related to the braid weave characteristics and material) are accounted for in the per-unit length transfer impedance Z_T and transfer admittance Y_T, and Z_c and Y_c are the per-unit length (series) self-impedance and (shunt) self-admittance formed by the inner conductor and the shield.

At this point, we rewrite the second differential equation in Eq. (A.1) in a generalized form that allows for cases when the braided cable is located within an arbitrary structure such as a metallic cavity of arbitrary shape. In other words, we recognize that there may be situations where the exterior voltage $V_0(z)$ is not easily defined. Relating the transfer admittance Y_T to the transfer capacitance C_T, we can write

$$\frac{dI_c}{dz} + Y_c V_c = -j\omega \tilde{C}_T q_0(z), \tag{A.2}$$

where $q_0(z)$ and $\tilde{C}_T$ represent the charge and capacitance (normalized by C_0) of the outer shield, respectively.

Using the current continuity equation $\frac{dI_0}{dz} = -j\omega q_0(z)$, Eq. (A.2) becomes

$$\frac{dI_c}{dz} + Y_c V_c = \tilde{C}_T \frac{dI_0(z)}{dz}\ . \tag{A.3}$$

Note that with the first differential equation in Eq. (A.1) and Eq. (A.3), the interior voltage and current can be found directly from the exterior cable current $I_0(z)$ (and its derivative) and the transfer parameters characterizing the braided shield.

To solve the interior system of equations (A.1) and (A.3), we will consider one source at a time and then apply a superposition of results for the final value of the inner conductor current. Thus,

assuming $J_z(z) = \tilde{C}_T \dfrac{dI_0(z)}{dz} = 0$ and using Eq. (A.1), the second-order differential equation for the inner conductor current becomes

$$\left(\frac{d^2}{dz^2} - \gamma_c^2\right) I_c = -Y_c E_z(z) = -Y_c Z_T I_0(z), \tag{A.4}$$

where $\gamma_c^2 = Z_c Y_c$. The solution of Eq. (A.4) is given by

$$\begin{aligned} I_{c,e}(z) &= \left[K_{1,e} + P_e(z)\right] e^{-\gamma_c z} + \left[K_{2,e} + Q_e(z)\right] e^{\gamma_c z} \\ V_{c,e}(z) &= \sqrt{\frac{Z_c}{Y_c}} \left\{ \left[K_{1,e} + P_e(z)\right] e^{-\gamma_c z} - \left[K_{2,e} + Q_e(z)\right] e^{\gamma_c z} \right\}, \end{aligned} \tag{A.5}$$

with $P_e(z) = \dfrac{1}{2}\sqrt{\dfrac{Y_c}{Z_c}} \int_{z_-}^{z} e^{\gamma_c z} E_z(z)\, dz$ and $Q_e(z) = \dfrac{1}{2}\sqrt{\dfrac{Y_c}{Z_c}} \int_{z}^{z_+} e^{-\gamma_c z} E_z(z)\, dz$, with $E_z(z) = Z_T I_0(z)$. The constants in Eq. (A.5) are determined from the terminating impedances $Z_{L,c}^-$ and $Z_{L,c}^+$ to the interior transmission line (at locations z_- and z_+, respectively, where $z_- < z < z_+$). More specifically,

$$\begin{aligned} K_{1,e} &= \rho_- e^{\gamma_c z_-} \frac{\rho_+ P_e(z_+) e^{-\gamma_c z_+} - Q_e(z_-) e^{\gamma_c z_+}}{e^{\gamma_c (z_+ - z_-)} - \rho_- \rho_+ e^{-\gamma_c (z_+ - z_-)}} \\ K_{2,e} &= \rho_+ e^{-\gamma_c z_+} \frac{\rho_- Q_e(z_-) e^{\gamma_c z_-} - P_e(z_+) e^{-\gamma_c z_-}}{e^{\gamma_c (z_+ - z_-)} - \rho_- \rho_+ e^{-\gamma_c (z_+ - z_-)}}, \end{aligned} \tag{A.6}$$

where the reflection coefficients at positions z_- and z_+ are $\rho_- = \dfrac{Z_{L,c}^- - \sqrt{\dfrac{Z_c}{Y_c}}}{Z_{L,c}^- + \sqrt{\dfrac{Z_c}{Y_c}}}$ and $\rho_+ = \dfrac{Z_{L,c}^+ - \sqrt{\dfrac{Z_c}{Y_c}}}{Z_{L,c}^+ + \sqrt{\dfrac{Z_c}{Y_c}}}$.

We now move on to accounting for the current contribution associated with the electric coupling of the exterior field. For this case, we assume $E_z(z) = 0$ so that we obtain

$$\left(\frac{d^2}{dz^2} - \gamma_c^2\right) V_c = -Z_c \tilde{C}_T \frac{dI_0(z)}{dz}, \tag{A.7}$$

and thus

$$
\begin{aligned}
V_{c,j}(z) &= \left[K_{1,j} + P_j(z)\right] e^{-\gamma_c z} + \left[K_{2,j} + Q_j(z)\right] e^{\gamma_c z} \\
I_{c,j}(z) &= \sqrt{\frac{Y_c}{Z_c}} \left\{ \left[K_{1,j} + P_j(z)\right] e^{-\gamma_c z} - \left[K_{2,j} + Q_j(z)\right] e^{\gamma_c z} \right\} ,
\end{aligned}
\tag{A.8}
$$

with $P_j(z) = \frac{1}{2}\sqrt{\frac{Z_c}{Y_c}} \int_{z_-}^{z} e^{\gamma_c z} J_z(z)\, dz$ and $Q_j(z) = \frac{1}{2}\sqrt{\frac{Z_c}{Y_c}} \int_{z}^{z_+} e^{-\gamma_c z} J_z(z)\, dz$, with $J_z(z) = \tilde{C}_T \frac{dI_0(z)}{dz}$, and

$$
\begin{aligned}
K_{1,j} &= \rho_- e^{\gamma_c z_-} \frac{Q_j(z_-) e^{\gamma_c z_+} + \rho_+ P_j(z_+) e^{-\gamma_c z_+}}{e^{\gamma_c (z_+ - z_-)} - \rho_- \rho_+ e^{-\gamma_c (z_+ - z_-)}} \\
K_{2,j} &= \rho_+ e^{-\gamma_c z_+} \frac{P_j(z_+) e^{-\gamma_c z_-} + \rho_- Q_j(z_-) e^{\gamma_c z_-}}{e^{\gamma_c (z_+ - z_-)} - \rho_- \rho_+ e^{-\gamma_c (z_+ - z_-)}} \quad .
\end{aligned}
\tag{A.9}
$$

The total current and voltage induced on the inner conductor is the sum of the two individual contributions (A.5) and (A.8):

$$
\begin{aligned}
I_c(z) &= I_{c,e}(z) + I_{c,j}(z) \\
V_c(z) &= V_{c,e}(z) + V_{c,j}(z) \quad .
\end{aligned}
\tag{A.10}
$$

DISTRIBUTION

Number	Mail Stop	Name	Dept.
1 (electronic)	MS0899	Technical Library	9536
3	MS1152	S. Campione	1352
3	MS1152	L. K. Warne	1352
1 (electronic)	MS1152	S. Campione	1352
1 (electronic)	MS1152	L. K. Warne	1352
1 (electronic)	MS1152	L. I. Basilio	1352
1 (electronic)	MS1152	L. San Martin	1352
1 (electronic)	MS1152	J. J. Himbele	1352
1 (electronic)	MS1152	I. C. Reines	1352
1 (electronic)	MS1152	A. Jones	1352
1 (electronic)	MS1152	R. A. Pfeiffer	1352
1 (electronic)	MS1152	A. J. Pung	1352
1 (electronic)	MS1152	B. Zinser	1352
1 (electronic)	MS1152	R. S. Coats	1352
1 (electronic)	MS1152	W. L. Langston	1352
1 (electronic)	MS1168	S. A. Hutchinson	1350


Sandia National Laboratories